Evaluating precipitation prediction skill for the Huanan pre- and post-rainy seasons in ECMWF subseasonal forecasts

Yanan Liu
changelyn@163.com
Jiangxi Academy of Sciences
Qiong Wu
Jiangxi Academy of Sciences
Yizhi Zhang
Jiangxi Academy of Sciences
Lujun Jiang
Jiangxi Academy of Sciences

Research Article

Keywords: Climate prediction, Prediction skill, Huanan pre- and post-rainy seasons in South China, General circulation

Posted Date: June 26th, 2023

DOI: https://doi.org/10.21203/rs.3.rs-3025427/v1

Version of Record: A version of this preprint was published at Geoscience Letters on March 5th, 2024. See the published version at https://doi.org/10.1186/s40562-024-00325-x.

Abstract

The rainy seasons in South China are divided into two phases according to the seasonal progression of the East Asian summer monsoon: the Huanan pre- and post-rainy seasons. The precipitation prediction skill for the two rainy seasons are investigated using subseasonal-to-seasonal (S2S) hindcast data from the European Centre for Medium-Range Weather Forecasts (ECMWF) for 2001–2019. The precipitation prediction skill and biases differ in the two rainy seasons, although some similar characteristics exist in regard to circulations and their influence on precipitation. During the two rainy seasons, the prediction skill of the circulation at 850 hPa in key areas is relatively high, and the circulation's influence on precipitation is well captured; additionally, the relationship between the circulation in key areas at 500 hPa and precipitation is less accurately constrained. Moreover, the precipitation prediction skill in the prerainy season is higher than that in the post-rainy season. The main bias is that the 200 hPa westerly provides favorable divergence conditions for prerainy season precipitation (pre-precipitation), while the post-rainy season precipitation (post-precipitation) displays almost no correlation with the circulation in the reanalysis product; however, the simulated circulation at 200 hPa is both tightly connected to the precipitation in the two rainy seasons, so the lower prediction skill in the post-rainy season is likely associated with overestimation of the complex physical mechanism of the upper-level circulation in the model.

1 Introduction

Huanan usually refers to the area south of 28°N and east of the Yunnan-Guizhou Plateau. The rainy season in the Huanan area lasts from April to September (Ramage, 1952), and both hourly and longer-scale heavy rainfall occur frequently (Luo et al., 2016; Zheng et al., 2016), resulting in high flash flood and urban waterlogging risks in South China (Hallegatte et al., 2013; Luo, 2017). With the seasonal progression of the East Asian summer monsoon circulation and precipitation, the rainy seasons in the Huanan area are often divided into two phases: the pre- and the post-rainy seasons (Li et al., 2011; Yuan et al., 2010). The Huanan prerainy season (April-June) is affected by large-scale systems accounting for approximately half of the total annual precipitation in China (Peng et al., 2006). In contrast, the Huanan post-rainy season (July-September) is mostly affected by complex tropical weather systems such as tropical cyclones and the intertropical convergence zone (ITCZ), which are comparatively unpredictable. Extreme precipitation events such as floods and droughts during the Huanan pre- and post-rainy seasons in South China have severely affected economic development and people's safety in China, so an accurate precipitation forecast for the rainy seasons is vital for disaster prevention.

Previous studies have investigated the atmospheric circulations that account for the interannual variations in the Huanan pre- and post-rainy seasons in South China. The precipitation anomalies during the Huanan pre- and post-rainy seasons are associated with the East Asian summer monsoon, including the western Pacific subtropical high (WPSH), upper-tropospheric subtropical East Asian jet stream, South Asian High (SAH) and cross-equatorial flow in Somalia and Australia (Ding et al., 2007; Liu and Ding, 2020; Zhang et al., 2003; Zhang and Tao, 1998). The interannual variations in the two rainy seasons can

be linked to atmospheric external forcing, such as the Eurasian teleconnection and thermal conditions in the Western Pacific (Ding and Wang, 2005; Nitta and Hu, 1996; Shi and Zhu, 1993; Wu et al., 2009; Zhang and Wu, 2011). Both rainy seasons are affected by the complex East Asian summer monsoon, which includes low-level and mid-to-high-level circulations (Chen et al., 2019). Due to differences in geographical location and monsoon stages, there are also differences in the contributions of low-latitude and mid-to-high-latitude circulations. Generally, low-latitude circulations are more predictable than those at mid-to-high latitudes (Ren et al., 2017; Wu et al., 2017). Consequently, it is necessary to further understand the predictability of precipitation in the two different rainy seasons.

The development of dynamic models has contributed to important advances in subseasonal to seasonal prediction (Saha et al., 2006, 2014; Vitart et al., 2017). Some models have shown reasonable skill in predicting the interannual variability of the Asian monsoon intensity (Jiang et al., 2013; Liu et al., 2014, 2015; Zhu and Shukla, 2013). Nevertheless, due to model error, predicting regional precipitation over China remains a great challenge for dynamical models (Liang et al., 2019; Liu et al., 2013, 2019), and the low prediction skill of these climate models is mainly associated with the fact that they cannot effectively simulate physical mechanisms. The subseasonal prediction skill of summer precipitation over eastern China is low, partly because the regional circulation cannot be well simulated or predicted in climate models (Zeng et al., 2012). In addition, some physical mechanisms in the model show discrepancies, and the impact of some key circulations on precipitation displays some notable deviations (Liu et al., 2021). Thus, understanding the differences in prediction skills and the corresponding causes is important for improving predictions.

In this study, the difference in the skill of predictions for the Huanan pre- and post-rainy seasons is analyzed. The ability of the model (the S2S dataset produced by the ECMWF) to predict the key circulation systems that affect precipitation in the two seasons and the corresponding relationships with precipitation are assessed. The possible reasons for the differences in the prediction skill between the two seasons are discussed. In Section 2, the data and methods are discussed. Section 3.1 presents the contrasting precipitation predictions for the Huanan pre- and post-rainy seasons and, the ability of the model to simulate the general circulations associated with precipitation in the Huanan pre- and post-rainy seasons is evaluated in Section 3.2, and the sources of prediction bias in the Huanan pre- and post-rainy seasons are discussed in Section 3.3. A Conclusions and discussion are given in Section 4.

2 Data and methods

2.1. Datasets

The subseasonal to seasonal prediction (S2S) database from 11 operational centers is useful for assessing predictions in the S2S time range. Considering the better forecasting ability of the ECMWF product (Lin, 2019), in the present analysis, we use ensemble forecasting data from the ECMWF. These data are obtained with the Integrated Forecasting System (IFS) version CY46R1. Operationally, the S2S dataset produced by the ECMWF is generated on the fly twice a week (Thursday and Monday). The

system provides daily ensemble forecasts of a wide variety of atmospheric variables (total precipitation, geopotential height, wind field, etc.) with a 46-day lead time. The reanalysis forecasts are used to calibrate the real-time forecasts by running an 11-member ensemble for the same start date as the 51-member real-time forecast but over the last 19 years for 2001–2019 and using the ERA-Interim product to establish the initial conditions. Additional details are available at https://confluence.ecmwf.int/display/S2S/ECMWF+Model. The reanalysis data used for model evaluation are the ERA-Interim daily precipitation and atmospheric variable data. The cumulative precipitation reanalysis product is produced in meters (m) at a 12-hour temporal step and is converted to millimeters (mm). More details are available at https://apps.ecmwf.int/datasets/data/interim-full-daily/levtype=sfc/.

Precipitation with a horizontal resolution of 1.0°×1.0° was used in both the model and reanalysis set, and the 500 hPa geopotential height with a horizontal resolution of 2.5°×2.5° was used.

2.2. Durations and areas of the two types of seasons

Following the relevant monitoring regulations of the China National Climate Center (NCC) and taking a comparative analysis of the rainy seasons into account, the same rainy season duration (5 weeks) is selected to study the difference in the precipitation prediction skill between the Huanan pre- (May 21 to June 20) and post- (July 13 to August 16) rainy seasons. Moreover, the Huanan area is located between 105 °–117 °E and 18 °– 27 °N.

2.3. Methods

The percentage anomaly between the reanalysis and predicted variables is defined as the departure from the multiyear mean climatologies for the two rainy seasons (2001 to 2019), calculated as follows:

$$DIFF\,(\%) = \frac{F - X}{X} \times 100$$

1

where *F* is the ensemble forecast value and *X* is the averaged reanalysis value.

The forecasting skill is assessed based on the anomaly correlation coefficient (ACC), the temporal correlation coefficient (TCC) and the root-mean-square error (RMSE).

$$ACC_j = \frac{\sum_{i=1}^{i=M}\left(\triangle x_{i,j} - \overline{\triangle x_j}\right) \times \left(\triangle \mathrm{y}_{i,j} - \overline{\triangle y_j}\right)}{\sqrt{\sum_{i=1}^{i=M}\left(\triangle x_{i,j} - \overline{\triangle x_j}\right)^2 \times \sum_{i=1}^{i=m}\left(\triangle y_{i,j} - \overline{\triangle y_j}\right)^2}}$$

2

$$TCC_i = \frac{\sum_{j=1}^{j=N}\left(x_{i,j} - \bar{\triangle x_i}\right) \times \left(y_{i,j} - \bar{\triangle y_i}\right)}{\sqrt{\sum_{j=1}^{j=N}\left(x_{i,j} - \bar{x_i}\right)^2 \times \sum_{j=1}^{j=N}\left(y_{i,j} - \bar{y_i}\right)^2}}$$

3

$$RMSE_i = \sqrt{\frac{\sum_{j=1}^{j=N}\left(\mathrm{x_{i,j}} - \mathrm{y_{i,j}}\right)^2}{N}}$$

4

where $x_{i,j}$and $y_{i,j}$ represent the reanalysis field and prediction field, respectively, i = 1,2,3..... M represents the grid number in the study region, and j = 1,2,3..... N represents the time series. Additionally, $\bar{\mathrm{x}}_{\mathrm{i}} = \frac{1}{\mathrm{N}}\sum_{\mathrm{j}=1}^{\mathrm{j}=\mathrm{N}} \mathrm{x_{i,j}}$,$\bar{\mathrm{y}}_{\mathrm{i}} = \frac{1}{\mathrm{N}}\sum_{\mathrm{j}=1}^{\mathrm{j}=\mathrm{N}} \mathrm{y_{i,j}}$,$\triangle \mathrm{x_{i,j}} = \mathrm{x_{i,j}} - \bar{\mathrm{x}}_{\mathrm{i}}$, and $\triangle \mathrm{y_{i,j}} = \mathrm{y_{i,j}} - \bar{\mathrm{y}}_{\mathrm{i}}$.

The definition of a blocking high is determined according to the regulations of the NCC for the real-time monitoring of blocking highs in the Northern Hemisphere, which is based on the height field gradient difference approach and was improved by Tibaldi and Molteni (Zhao, 2000). A certain longitude index can be calculated as follows:

$$GHG = \frac{Z(_1) - Z(_2)}{_1 - _2}$$

5

where *Z* is the geopotential height, $_1$ and $_2$ are latitudes, $_1$= 60+δ, and $_2$=40+δ. In this case, *δ* can be −5, 0, or 5. The blocking high in a certain key area is the average blocking pressure within the longitude interval of the key area.

The Eurasian teleconnection (EU) index can be defined as follows:

$$I = -0.25Z^*_{(60^\circ\mathrm{N},20^\circ\mathrm{E})} + 0.5Z^*_{(62.5^\circ\mathrm{N},60^\circ\mathrm{E})} - 0.25Z^*_{(60^\circ\mathrm{N},110^\circ\mathrm{E})}$$

6

where $Z' = Z - \overline{Z}$, $Z^* = Z'\sin 45^\circ / \sin\phi$, Z is the 500 hPa geopotential height, $\overline{Z}$ is the climatological mean of the 500 hPa geopotential height, and is the latitude (Wallace and Gutzler, 1981).

Regression analysis is used to assess the relationship between an outcome variable and one or more factors or confounding variables, and correlation analysis is used to test the significance of the relationship.

3 Result

3.1. Skill of precipitation predictions between the Huanan pre- and post-rainy seasons

The skill of precipitation predictions between the Huanan pre- and post-rainy seasons was compared, and Fig. 1 shows the ACC distributions for the ERA data and ECMWF predictions for different lead times and ensemble-averaged forecasts. Forecasts beginning at each start time are run for total precipitation during the Huanan pre- (May 21 to June 20) and post- (July 13 to August 16) rainy seasons. For example, forecasts for the Huanan rainy season with a 0-day lead time represent the total precipitation from May 21 to June 20 and are initialized on May 21, and those with a 3-day lead time are similar but are initialized on May 18. By comparing forecasts with different lead times (0, 3, 7 and 10 days ahead), it is found that the precipitation forecasting skill is better for the prerainy season than for the post-rainy season for lead times of 0, 3, and 7 days (Fig. 1a). The ACC is the best for the 0-day lead time, and the multiyear average ACC is 0.26 for the prerainy season and 0.08 for the post-rainy season. The decrease in ACC is associated with an increase in lead time, although the rate of the decrease varies for each season. Based on the ensemble forecasts of 51 members with lead times of 0, 3, and 7 days (for the similar skill in the prerainy season of 10-day lead time), obvious interannual differences are observed in the precipitation forecasting skill in the two seasons (Fig. 1b). The precipitation forecasting skill during the prerainy season for 2001–2019 is generally better than that in the post-rainy season. From the multiyear averages, the ACC of the ensemble forecast is 0.30 during the prerainy season and 0.09 during the post-rainy season. That is, there are obvious differences between the two rainy seasons in terms of the skill of ensemble precipitation forecasts.

Considering the number of samples, in the following analysis, the rainy season predictions for 51 members with lead times of 0, 3, and 7 days (the same 51 members at each lead time) initialized with slightly different atmospheric initial conditions are used.

Diff (Fig. 2a and d) is defined as the difference between the modeled and reanalysis precipitation values in the two rainy seasons. During the prerainy season, precipitation is 20–40% higher in the central and northern parts of Guangdong and Guangxi, 20–60% higher in the Beibu Gulf region, and 20–40% lower in Hainan and the adjacent sea areas than in the post-rainy season. In the post-rainy season, precipitation is 20–40% lower in most areas than it is during the prerainy season. The RMSE of total precipitation in the two rainy seasons (Fig. 2b and e) is comparatively larger in the prerainy season (reaching 130–160 mm in the center) and smaller in most areas in the post-rainy season (generally 100–130 mm). This is likely related to the higher precipitation in the prerainy season than in the post-rainy season. From the TCC between the reanalysis and model-predicted precipitation values in the two rainy seasons (Fig. 2c and f), there are obvious differences in different areas in the prerainy season. Specifically, the forecasting skill is best in Hainan and the adjacent areas, and in most areas with TCCs between 0.4 and 0.7, the forecasts are significantly accurate at the 95% confidence level. In general, the TCC is low in the post-rainy season,

with weak TCCs of 0.1–0.3 in most areas, and the forecasts in almost all areas are not significant at the 95% significance level.

3.2. Prediction of general circulation associated with precipitation during the Huanan pre- and post-rainy seasons

3.2.1. The Huanan rainy season

Figure 3 shows a conceptual map of large-scale climatological circulations during the Huanan rainy season. At 500 hPa, the Lake Baikal high is blocked, and the stable East Asia low trough extends from the south of the blocking high to the middle latitudes; these systems are advantageous for bringing cold air to the north of the Huanan area and for promoting interactions with the East Asian summer monsoon (Ding et al., 2020), while the WPSH is distributed zonally above the ocean to the east of Taiwan and south of Japan. Huanan is located at the bottom of the East Asian trough and northwest of the WPSH, forming a favorable situation of “high in the east and low in the west” at 850 hPa, and the southwesterly prevails over South China. Moreover, the 200 hPa SAH moves to the Indo-China Peninsula with the upper-level westerly covering Huanan, thus providing the upper-level divergent conditions for heavy rainfall during the prerainy season.

According to the synoptic model shown above, the responses of the circulations at different levels to precipitation in the prerainy season are further analyzed. To identify the key areas of circulation at 500 hPa that affect precipitation, the reanalysis (model-predicted) precipitation index is used to regress the reanalysis (model-predicted) 500 hPa geopotential height. The regressed reanalysis field (Fig. 4a) indicates that the positive areas are located in high-latitude regions, such as that near Lake Baikal, and the negative areas are located in middle-latitude areas from Mongolia to Inner Mongolia, which highlights the positive influence of the active trough on precipitation. The regressed geopotential height at high and middle latitudes is basically consistent with that based on the reanalysis product (Fig. 4d), and the regression is positive, negative and positive from high to low latitudes.

Furthermore, the reanalysis (modeled) precipitation index is used to regress the reanalysis (modeled) 850 hPa wind field. The regressed reanalysis field (Fig. 4b) indicates that the areas that passed the significance level are mainly located in Southmost China (southwesterly) and northernmost China (southeasterly). However, the significant regression areas are distributed from high to low latitudes in the regressed model field (Fig. 4e): the Japan Sea, the Huaihe River Basin and the South China Sea line along the eastern coast of China, especially the anticyclonic circulation in South China that contributes to southwesterlies prevailing over Huanan. Finally, the key areas of high-level circulation during the prerainy season are analyzed, and the northern Huanan areas (westerlies) and low-latitude areas from the South China Sea to the tropical western Pacific (northeasterly) display significant circulations in the regressed reanalysis field (Fig. 4c). In the regressed model field (Fig. 4f), the circulations north of Huanan (westerly) are relatively significant, although small in size. In brief, northern Huanan’s significant westerlies at 200

hPa in both the reanalysis and modeled fields maintain upper-level divergence conditions for rainfall in South China.

Based on the above analysis, the low-, middle- and high-level circulation indices are obtained in turn. First, the effects of two key circulation configurations (the high-latitude blocking high pressure (BHP) and geopotential height anomaly over middle-latitude ocean areas at 500 hPa) on precipitation during the prerainy season are discussed. According to the reanalysis products and model performance, δ is set to -5 in formula 5 for the BHP. The geopotential height difference between the two different latitudes in the longitude range from the east of Lake Baikal to the Okhotsk Sea (110°–140° E; the area between the lines in Fig. 5a and c) is selected to represent the BHP in this key area. Figure 5a shows the 500 hPa height anomaly field regressed from the BHP in the reanalysis product. In the central area, a single BHP can be observed. The model regression result also highlights key areas, and the "+ −" distribution in the high and middle latitudes is significant (Fig. 5c). In the reanalysis precipitation field regressed based on BHP, a significant positive center is found in the south, and a negative correlation is observed in a small part of the north (Fig. 5b). In the model precipitation field regressed based on the BHP, northern Huanan is the center of the positive area, and the magnitude gradually decreases from the center, although not significantly at the 95% significance level (Fig. 5d).

To discuss the effect of the low-level 850 hPa wind anomaly on precipitation during the prerainy season, the significant positive area is selected from the most obvious southwesterly area (15°–20°N, 100°–110°E) in Fig. 4b, e. The 850 hPa wind index (U850) is the average zonal wind anomaly within the study area (black box in Fig. 6a and c). Figure 6a and c show the 850 hPa wind distribution regressed based on U850 in the reanalysis and model sets, respectively. The indices both effectively highlight the key areas with anomalous southwesterlies in South China. In the reanalysis precipitation field regressed with U850 (Fig. 6b), significant positive areas can be seen across all of Huanan and the adjacent sea. In the regression field of modeled precipitation based on U850 (Fig. 6d), the overall distribution of precipitation is similar to that in the reanalysis regression field. However, the results are significant in comparatively fewer regions.

Ding et al. (2011) and Du and Chen (2019) believe that the interaction between the upper-level westerly jet and the low-level southwesterly jet during the prerainy season in South China is significant, which can be conducive to the coupling of the upper- and low-level jets to facilitate the occurrence of heavy rain in Huanan. Combined with the significant response areas in Fig. 4c and f, the 200 hPa wind index (U200) is constructed as the average 200 hPa zonal wind anomaly in the area (22.5°–30°N, 110°–120°E, black box in Fig. 7a and c) and is standardized to regress the 200 hPa wind anomaly field (Fig. 7a), which displays an eastern-western-eastern zonal wind distribution in the high (40°N), middle (30°N), and low (10°N) latitudes, respectively. The regression field of the model displays a similar distribution along the high (45°N), middle (35°N) and low (15°N) latitudinal belts, with values passing the 95% confidence test in both cases (Fig. 7c). In the reanalysis precipitation field regressed based on U200, there is a significant positive center in the western part of the region (Fig. 7b). In the regressed field of modeled precipitation,

the positive significant center is along the northern boundary of Guangxi (Fig. 7d), and the values in relatively few regions passed the significance test.

3.2.2. The Huanan post-rainy season

Previous studies have shown that the zonal “+ − +” wave train structure in the Ural Mountains of Eurasia, the area between Lake Balkhash and Lake Baikal, and the area from Bohai Bay to the Japanese archipelago is conducive to reducing precipitation in Huanan. Wei et al. (2003) and Wang and He (2015) called this wave train the EU teleconnection pattern. To analyze the key areas of circulation affecting precipitation in the Huanan post-rainy season, the reanalysis (model-predicted) precipitation index is used to regress the reanalysis (model-predicted) 500 hPa height field. The regressed field (Fig. 8a) indicates that the regressions over the Nordic continent and in the Ural Mountains, the Baikal region, and the Sea of Okhotsk display “+ − + −” wave trains, similar to the EU pattern. In the regressed model field (Fig. 8d), similar “− + −” wave train distributions can be seen in the Ural Mountains, Northeast China and the Sea of Okhotsk, but the positive center above the Nordic continent disappears.

Combined with the significant response areas in Fig. 8a, the EU index is constructed (Formula 6) and is standardized to regress the reanalysis (model-predicted) 500 hPa height anomaly field (Fig. 8b and e). The comparable high-latitude fields show similar anomalous positive distributions above the Ural Mountains and the Sea of Okhotsk and negative distributions from Lake Baikal to the Siberian Plain, which are contrary to the distribution of key areas in the 500 hPa height field regressed based on precipitation index, but both pass the 95% confidence test. At middle latitudes, the negative areas are both nonsignificant. In the reanalysis precipitation field regressed based on the EU product, there is a negative anomaly in most areas that is significant (Fig. 8c), and significant negative areas are uncommon in the regressed field of model precipitation (Fig. 8f). There is a difference between the reanalysis and model results in terms of the significant relationship between EU and precipitation in the Huanan rainy season.

As in Figs. 6a, c, Figs. 9a and c show the regression between the 850 hPa wind index (U850) and the 850 hPa wind field anomaly but in the post-rainy season; in both subfigures, key areas with significant anomalous southwesterlies at 850 hPa can be observed over the South China Sea. Then, in the reanalysis precipitation field regressed based on U850 (Fig. 9b), a significant positive anomaly can be seen over Huanan, except near northeastern Guangdong. In the modeled precipitation field regressed based on U850 (Fig. 9d), the overall distribution of precipitation is similar to that obtained with reanalysis regression. However, the values were significant in comparatively more regions.

The distribution of the regression between U200 and the corresponding wind field anomalies in the Huanan post-rainy season is shown in Fig. 10a and c. The regression field of the model (Fig. 10c) illustrates the distribution of the latitudinal wind belts at high (40°N)-middle (30°N)-low (10°N) latitudes, all passing the 95% confidence test, while no areas display significant values in the reanalysis regression field (Fig. 10a). Moreover, Huanan was influenced the upper-level westerly divergence condition in the

model, but there was no signal in the reanalysis product. In the modeled precipitation field regressed with U200 (Fig. 10d), the positive center in the northwestern region generally passes the significance test; however, the positive anomalies with small magnitudes in Guangxi are generally nonsignificant in the reanalysis regression field.

Based on the above analysis, there is a large difference between the reanalysis and model results regarding the relationship between U200 and precipitation in the Huanan post-rainy season, revealing that the physical mechanisms of the upper-level wind and precipitation in the model are likely overestimated. To further study the relationship between upper-level circulation and precipitation during the Huanan post-rainy season, the precipitation index is used to regress the vertical cross-section of the meridional wind field along 117°E (Fig. 11). The anomalous southerlies in central Huanan extend from the near-surface levels to the upper levels at 200 hPa and are significant at all levels in the modeled vertical cross-section of the wind field (Fig. 11b); additionally, significant southerly anomalies only exist at low levels in the reanalysis regression field (Fig. 11a), which further indicates that the physical mechanisms of upper-level wind and precipitation in the model are different and overestimated.

3.3. Sources of prediction bias between the Huanan pre- and post-rainy seasons

The difference in circulation in the model will inevitably lead to different simulation effects when estimating the circulation index in each key area. As shown in Table 1, the simulation effect of the BHP index at 500 hPa is the best, and the corresponding correlation coefficient with the reanalysis product is 0.63; additionally, the correlation coefficient with U850 is 0.59, and the simulation effect for U200 is comparatively worse (correlation coefficient of 0.41). Thus, the three indices at low, middle and high atmospheric levels, with correlation coefficients from 0.4–0.6, are reasonable during the prerainy season. The simulation effect based on the U850 index in the post-rainy season is best, with a correlation coefficient of 0.76, and the EU simulation effect is good, with a coefficient of 0.59. Similar to those in the prerainy season, the key areas of the 500 hPa and 850 hPa circulation indices in the post-rainy season are effectively simulated, with correlation coefficients of 0.6–0.8, and the coefficient for U200 is 0.2. Notably, the U200 index is constructed as the average 200 hPa zonal wind anomaly in the same area (black box in Fig. 7a and c) and is used to constrain the upper-level circulation conditions, even though there are no areas with significant values in the reanalysis set.

Table 1. Correlations between indices for ERA-Interim and ECMWF predictions.

Huanan prerainy season			Huanan post-rainy season		
BHP	U850	U200	EU	U850	U200
0.63	0.59	0.41	0.59	0.76	0.20

The relationship between the circulation index in the two rainy seasons and precipitation in the key areas in the reanalysis product and model results is further analyzed (Table 2). The correlation coefficient values between the BHP index and precipitation at 500 hPa during the prerainy season reach 0.61 and

0.35 for the ERA-Interim and ECMWF predictions, respectively. The correlation coefficients between the U850 index and precipitation are the highest (0.85 and 0.78), and values of 0.54 and 0.45 are obtained between the U200 index and precipitation. The relationships between the indices and precipitation in the reanalysis and model sets are consistent. In the post-rainy season, the relationship between precipitation and the EU index at 500 hPa displays an opposite relationship with negative coefficients (-0.51 and −0.30), and the coefficients between the U850 index and precipitation are 0.63 and 0.56, respectively. For the reanalysis product, the correlation coefficient between the U200 index and precipitation is 0.20 and not significant. However, the correlation coefficient reaches 0.58 for the model results. The physical mechanism of the 200 hPa in the post-rainy season is overestimated by the model in key areas, contributing to the lower precipitation prediction skill in the post-rainy season.

Table 2. Correlations between indices and precipitation for ERA-Interim and ECMWF predictions.

Correlation / Index	Huanan prerainy season			Huanan post-rainy season		
	BHP	U850	U200	EU	U850	U200
Index.ERA & P.ERA	**0.61**	**0.85**	**0.54**	**-0.51**	**0.63**	**0.20**
Index.S2S & P.S2S	**0.35**	**0.78**	**0.45**	**-0.30**	**0.56**	**0.58**

4 Conclusions and discussion

In this study, the interannual skill of precipitation prediction in the Huanan pre- and post-rainy seasons in South China is evaluated using reanalysis data (ERA-Interim) and ECMWF-S2S hindcast data for 2001–2019. In most years, the precipitation prediction skill is higher during the prerainy season than during the post-rainy season in South China. During the Huanan rainy season, the TCC in most of the region reaches between 0.4 and 0.7. However, the TCC in most of the central region is below 0.2 in the Huanan post-rainy season.

The precipitation prediction skill and corresponding bias differ in the two rainy seasons, and some similar characteristics exist in terms of the simulated circulations and their influence on precipitation. During the two rainy seasons, the skill of circulation prediction at low levels (850 hPa) is high, and the relationship between circulations and precipitation is well captured. However, the prediction skill for circulations at middle levels (500 hPa) in key areas is relatively good, although the relationship between circulations and precipitation in key areas are less skillful in model in the two rainy seasons.

Model biases are observed in the circulation simulation and its influence on precipitation at high levels (200 hPa). In the Huanan prerainy season, the response to the upper level westerly in certain areas is strong, the 200 hPa circulation is well simulated, and the response of precipitation to U200 is effectively reflected in the model. During the Huanan post-rainy season, the prediction of the circulation at 200 hPa is not captured, but the response of postprecipitation to U200 is fairly strong in the model. The main bias is that the 200 hPa westerly provides favorable divergence conditions for the prerainy period, but circulations are not present for the post-rainy period in the reanalysis product. During the two rainy seasons, the simulated 200 hPa circulations are tightly connected to the corresponding precipitation, and

the lower prediction skill in the post-rainy season is likely due to the overestimation of the physical mechanism of the upper-level circulation in the model.

Numerical models inevitably have errors. It is becoming increasingly difficult to improve models to further increase their forecasting skill (Feng et al., 2013; Ren, 2006; Saha, 1992; Zheng et al., 2009). Many studies have used statistical methods to improve the forecasting ability of dynamic models (Feddersen and Andersen, 2005; Guo and Li, 2012; Wei and Huang, 2010), but the objective is to understand the sources of bias in these models. In this paper, the difference in precipitation predictability in the Huanan pre- and post-rainy seasons is discussed. The sources of bias in the two periods are analyzed, and the findings have important implications for the localized interpretation of models in the future. During the two rainy seasons, more attention should be given to the physical mechanisms associated with circulation and precipitation in key areas. Especially in the post-rainy season, it is necessary to conduct statistical analyses of the upper-level circulation fields and surface precipitation in reanalysis products, and inappropriate physical effects should be removed. Therefore, it is necessary to explore the specific physical mechanisms of models to predict precipitation in different rainy seasons in future work.

Abbreviations

Subseasonal-to-seasonal (S2S); the European Centre for Medium-Range Weather Forecasts (ECMWF); prerainy season precipitation (pre-precipitation); postrainy season precipitation (post-precipitation); the anomaly correlation coefficient (ACC); the temporal correlation coefficient (TCC) ; the root-mean-square error (RMSE);the intertropical convergence zone (ITCZ); the western Pacific subtropical high (WPSH); South Asian High (SAH); the blocking high pressure (BHP); the Eurasian teleconnection (EU)

Declarations

Ethics approval and consent to participate: Not applicable.

Consent for publication: Not applicable.

Funding: This work is supported by the National Natural Science Foundation of China (41765001).

Competing interests: The authors declare no conflicts of interest.

Availability of data and material: The authors confirm that the data supporting the findings of this study are available within the article manuscript.

Acknowledgements:

The authors thank the ECMWF for providing the S2S data used in this study and are extremely grateful to the anonymous reviewers for their valuable comments on this paper.

Authors' contributions and information

Yanan Liu.

Meteorological Sciences Institute, Jiangxi Meteorological Bureau, Nanchang, 330046, China. performed the research, analysed data, and wrote the paper.

E-mail: changelyn@163.com

Qiong Wu.

Climate Center, Jiangxi Meteorological Bureau, Nanchang, 330046,China.contributed the central idea and collected the data.

E-mail: wuqioong@foxmail.com

Yizhi Zhang.

Meteorological Sciences Institute, Jiangxi Meteorological Bureau, Nanchang, 330046, China.contributed to refining the ideas and finalizing this paper.

E-mail: Meteorologist@sina.com

Lujun Jiang.

Meteorological Sciences Institute, Jiangxi Meteorological Bureau, Nanchang, 330046, China.discussed the results.

E-mail: jlj0629@ 163. com

***Corresponding author**: Dr.Yanan Liu, Meteorological Sciences Institute, Jiangxi Meteorological Bureau, 323 Aixihu Road, Gaoxin District, Nanchang 330046, China.

E-mail: changelyn@163.com

Tel:15261826321

References

1. Chen, L., Zhao, J., Gu, W., et al., 2019. Advances of research and application on major rainy seasons in China. J. Appl. Meteorol. Sci. 30, 385–400. https://doi.org/10.11898/1001-7313.20190401.
2. Ding, Q., Wang, B., 2005. Circumglobal teleconnection in the northern hemisphere summer. J. Clim. 18, 3483–3505. https://doi.org/10.1175/jcli3473.1.
3. Ding, Y., Liang, P., Liu, Y., et al., 2020. Multiscale variability of meiyu and its prediction: a new review. J. Geophys. Res. Atmos. 125, e2019JD031496. https://doi.org/10.1029/2019jd031496.

4. Ding, Y.H., Liu, C.H., Shen, X.Y., 2011. Statistical analysis of the relationship among warm sector heavy rainfall, upper and lower tropospheric jet stream and South Asia High in May and June from 2005 to 2008. J. Trop. Meteorol. 27, 307–316.
5. Ding, Y.H., Liu, J.J., Sun, Y., 2007. A study of the synoptic-climatology of the Meiyu system in East Asia. J. Atmos. Sci. 31, 1082–1101.
6. Du, Y., Chen, G., 2019. Heavy rainfall associated with double low-level jets over Southern China. Part II: convection initiation. Mon. Weather Rev. 147, 543–565. https://doi.org/10.1175/mwr-d-18-0102.1.
7. Feddersen, H., Andersen, U., 2005. A method for statistical downscaling of seasonal ensemble predictions. Tellus A 57, 398–408. https://doi.org/10.1111/j.1600-0870.2005.00102.x.
8. Feng, G., Zhao, J., Zhi, R., et al., 2013. Recent progress on the objective and quantifiable forecast of summer precipitation based on dynamical-statistical method. J. Appl. Meteorol. Sci. 24, 656–665.
9. Guo, Y., Li, J.P., 2012. A time-scale decomposition statistical downscaling model: case study of North China rainfall in rainy season. Chin. J. Atmos. Sci. 36, 385–396.
10. Hallegatte, S., Green, C., Nicholls, R.J., et al., 2013. Future flood losses in major coastal cities. Nat. Clim. Change 3, 802–806. https://doi.org/10.1038/nclimate1979.
11. Jiang, X., Yang, S., Li, Y., et al., 2013. Seasonal-to-interannual prediction of the Asian summer monsoon in the NCEP climate forecast system version 2. J. Clim. 26, 3708–3727. https://doi.org/10.1175/jcli-d-12-00437.1.
12. Li, X.M., Yang, Y.J., He, L.Y., 2011. Relationship between the first rainy season precipitation anomaly in South China and atmospheric circulation. J. Meteorol. Res. Appl. 32, 109–110.
13. Liang, P., Hu, Z.Z., Liu, Y., et al., 2019. Challenges in predicting and simulating summer rainfall in the eastern China. Clim. Dyn. 52, 2217–2233. https://doi.org/10.1007/s00382-018-4256-6.
14. Lin, Q., 2019. Performance of sub-seasonal to seasonal (S2S) products for global precipitation forecasts. J. Water. Resour. Res. 8(6):547–556. https://doi.org/10.12677/JWRR.2019.86062.
15. Liu, X., Wu, T., Yang, S., et al., 2015. Performance of the seasonal forecasting of the Asian summer monsoon by BCC_CSM1.1(m). Adv. Atmos. Sci. 32, 1156–1172. https://doi.org/10.1007/s00376-015-4194-8.
16. Liu, X., Wu, T., Yang, S., et al., 2014. Relationships between interannual and intraseasonal variations of the Asian-western Pacific summer monsoon hindcasted by BCC_CSM1.1(m). Adv. Atmos. Sci. 31, 1051–1064. https://doi.org/10.1007/s00376-014-3192-6.
17. Liu, Y., Hong, J., Liu, C., et al., 2013. Meiyu fooding of Huaihe river valley and anomaly of seasonal variation of subtropical anticyclone over the Western Pacifc. Chin. J. Atmos. Sci. 37, 439–450.
18. Liu, Y., Ke, Z., Ding, Y., 2019. Predictability of East Asian summer monsoon in seasonal climate forecast models. Int. J. Climatol. 39, 5688–5701. https://doi.org/10.1002/joc.6180.
19. Liu, Y.Y., Ding, Y.H., 2020. Characteristics and possible causes for the super Meiyu in 2020. Meteorol. Mon. 46, 1393–1404.

20. Liu, Y., Hu, Z.Z., Wu, R., et al., 2021. Subseasonal prediction and predictability of summer rainfall over eastern China in BCC_AGCM2.2. Clim. Dynam. 56(7):2057–2069.
21. Luo, Y., 2017. Advances in understanding the early-summer heavy rainfall over South China, in: Chang, C.P., Lau, N.G., Johnson, R.H., Wang, B., Wheeler., M., World Scientife Series on Asia-Pacific Weather and Climate, 9, 215–226.
22. Luo, Y., Wu, M., Ren, F., et al., 2016. Synoptic situations of extreme hourly precipitation over China. J. Clim. 29, 8703–8719. https://doi.org/10.1175/jcli-d-16-0057.1.
23. Nitta, T., Hu, Z.Z., 1996. Summer climate variability in China and its association with 500 hPa height and tropical convection. J. Meteorol. Soc. Jpn. II 74, 425–445. https://doi.org/10.2151/jmsj1965.74.4_425.
24. Peng, L.Y., Wang, Q.Q., Ma, H., 2006. A study on the climatic features of the rainfall of rain storms in the pre-flood season in South China. J. NangJing Inst. Meteorlogy 29, 249–253.
25. Ramage, C. S., 1952. Variation of rainfall over South China through the wet season. Bull. Amer. Meteor. Soc. 33, 308–311.
26. Ren, H. L., 2006. Strategies and methods for dynamic similarity forecasting, in: Lanzhou, Lanzhou University.
27. Saha, S., 1992. Response of the NMC MRF model to systematic error correction within integration. Mon. Weather Rev. 120, 345–360. https://doi.org/10.1175/1520-0493(1992)120<0345:ROTNMM>2.0.CO;2.
28. Saha, S., Moorthi, S., Wu, X., et al., 2014. The NCEP climate forecast system version 2. J. Clim. 27, 2185–2208. https://doi.org/10.1175/jcli-d-12-00823.1.
29. Saha, S., Nadiga, S., Thiaw, C., et al., 2006. The NCEP climate forecast system. J. Clim. 19, 3483–3517. https://doi.org/10.1175/jcli3812.1.
30. Shi, N., Zhu, Q.G., 1993. Studies on the northern early summer teleconnection patterns, their interannual variations and relation to drought/flood in China. Adv. Atmos. Sci. 10(2): 155–168.
31. Vitart, F., Ardilouze, C., Bonet, A., et al., 2017. The subseasonal to seasonal (S2S) prediction project database. Bull. Am. Meteorol. Soc. 98, 163–173. https://doi.org/10.1175/BAMS-D-16-0017.1.
32. Wallace, J.M., Gutzler, D.S., 1981. Teleconnections in the geopotential height field during the Northern Hemisphere Winter. Mon. Weather Rev. 109, 784–812. https://doi.org/10.1175/1520-0493(1981)109<0784:titghf>2.0.co;2.
33. Wang, H., He, S., 2015. The North China/Northeastern Asia severe summer drought in 2014. J. Clim. 28, 6667–6681. https://doi.org/10.1175/jcli-d-15-0202.1.
34. Wei, F.Y., Huang, J.Y., 2010. A study of predictability for summer precipitation on east China using downscaling techniques. J. Trop. Meteorol. 26, 483–488.
35. Wei, J., Zhang, Q.Y., Tao, S.Y., 2003. Characteristics of atmospheric circulation anomalies during persistent droughts in North China for last two decades. J. Appl. Meteorol. Sci. 14, 140–151.

36. Wu, B., Zhang, R., Wang, B., 2009. On the association between spring Arctic sea ice concentration and Chinese summer rainfall: a further study. Adv. Atmos. Sci. 26, 666–678. https://doi.org/10.1007/s00376-009-9009-3.
37. Wu, J., Ren, H., Zhang, S., et al., 2017. Evaluation and predictability analysis of seasonal prediction by BCC second-generation climate system model. Chin. J. Atmos. Sci. 41, 1300–1315. https://doi.org/10.3878/j.issn.1006-9895.1703.16256.
38. Yuan, F., Wei, K., Chen, W., et al., 2010. Temporal variations of the fontal and monsoon storm rainfall during the first rainy season in South China. Atmos. Ocean. Sci. Lett. 3, 243–247. https://doi.org/10.1080/16742834.2010.11446876.
39. Zeng, G., Wang, W.C., Shen, C., 2012. Association of the rainy season precipitation with low-level meridional wind in the Yangtze River valley and North China. J. Clim. 25:792–799. https://doi.org/10.1175/JCLI-D-10-05027.1
40. Zhang, Q., Tao, S., Zhang, S., 2003. The persistent heavy rainfall over the Yangtze River valley and its associations with the circulations over East Asian during summer. J. Atmos. Sci. 27, 1018–1103.
41. Zhang, Q.Y., Tao, S.Y., 1998. Influence of Asian mid-high latitude circulation on East Asian summer rainfall. Acta Meteorol. Sin. 56, 199–211.
42. Zhang, R.N., Wu, B.Y., 2011. The Northem Hemisphere atmospheric response to spring Aretic sea ice anomalies in CAM3. 0 model. Chin. J. Atmos. Sci. 35, 847–862.
43. Zhao, Z.G., 2000. Summer Drought, Flood and Environmental Field in Summer of China. China Meteorological Press, Beijing.
44. Zheng, Y., Xue, M., Li, B., et al., 2016. Spatial characteristics of extreme rainfall over China with hourly through 24-hour accumulation periods based on national-level hourly rain gauge data. Adv. Atmos. Sci. 33, 1218–1232. https://doi.org/10.1007/s00376-016-6128-5.
45. Zheng, Z.H., Ren, H.L., Huang, J.P., 2009. Analogue correction of errors based on seasonal climatic predictable components and numerical experients. Acta. Phys. Sin. 58(10):7359-7367.
46. Zhu, J., Shukla, J., 2013. The role of air–sea coupling in seasonal prediction of asia–pacific summer monsoon rainfall. J. Clim. 26, 5689–5697. https://doi.org/10.1175/jcli-d-13-00190.1.

Figures

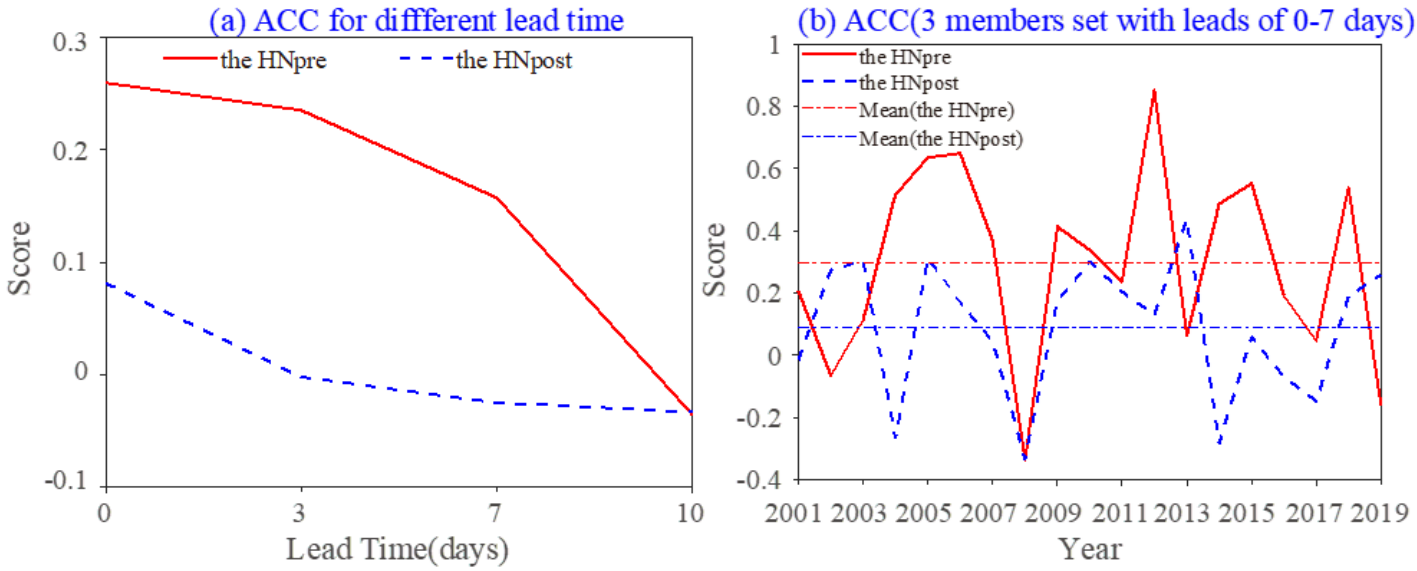

Figure 1

ACCs between ERA-Interim and ECMWF predictions in the Huanan pre- and post-rainy seasons: (a) with lead times of 0, 3, 7 and 10 days; (b) time series from 2001 to 2019.

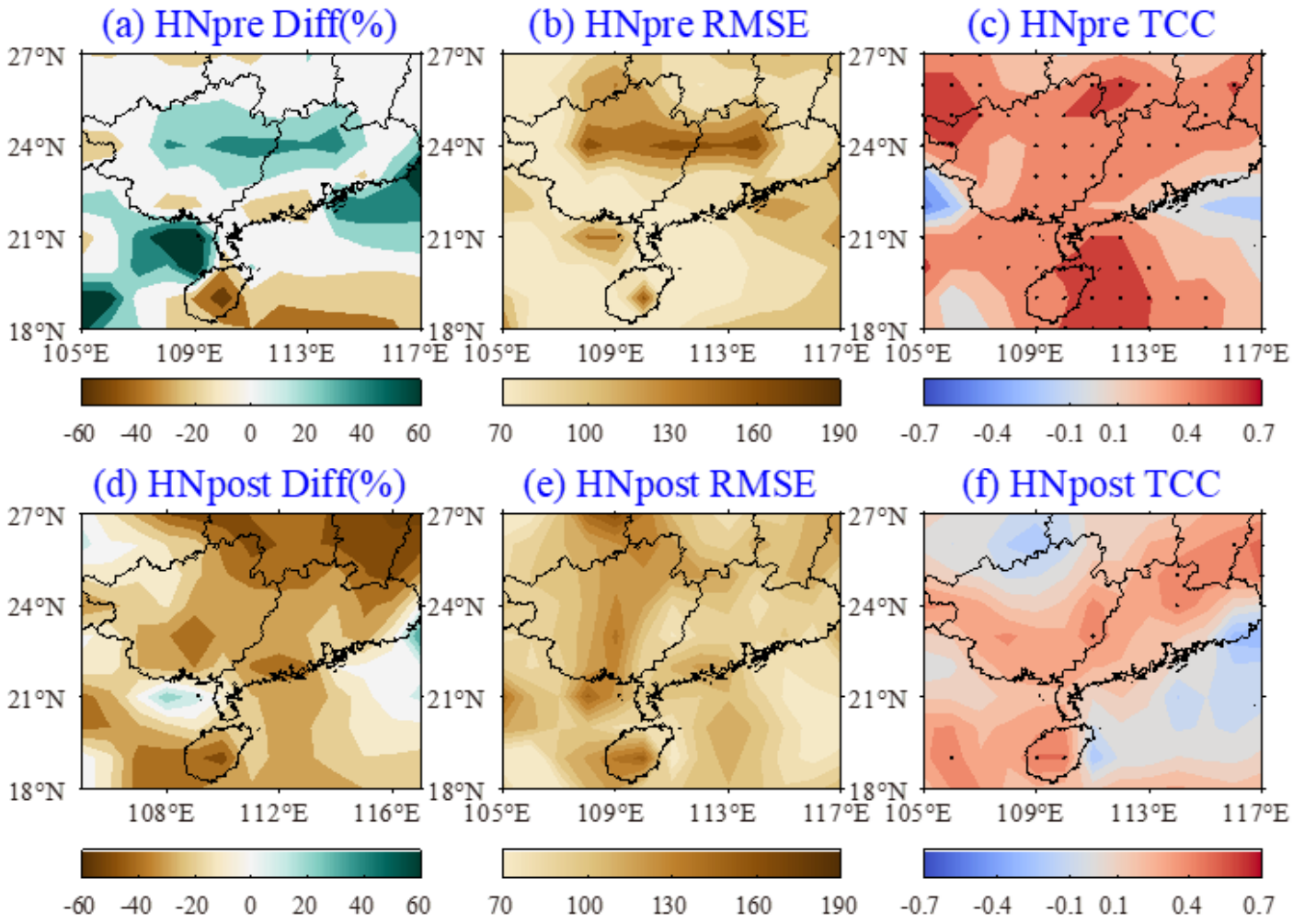

Figure 2

DIFFs (%), RMSEs, and TCCs derived between the ERA-Interim and ECMWF precipitation series during the (a-c) Huanan prerainy season and (d-f) post-rainy season for 2001-2019. The dots represent significance at the 95% confidence level in (c) and (f).

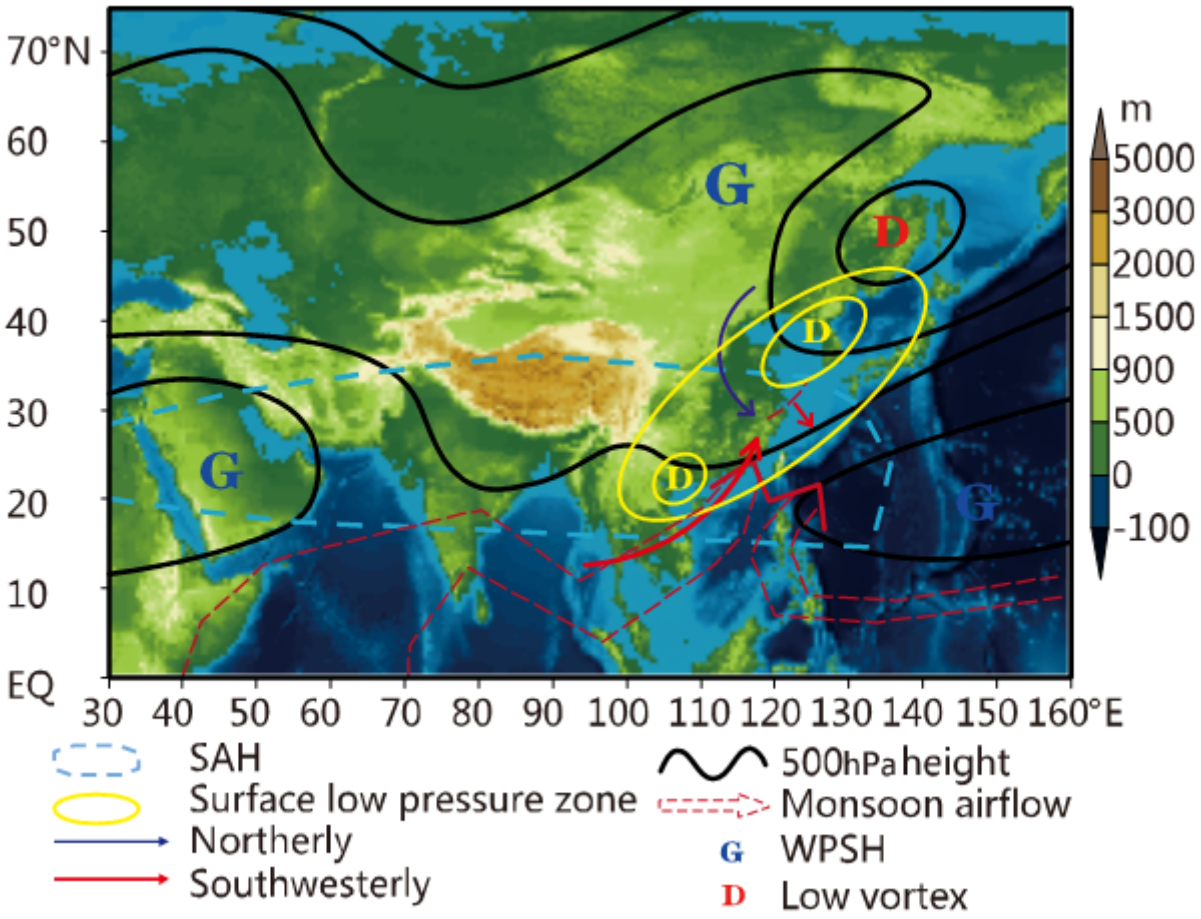

Figure 3

Conceptual map of large-scale circulations during the Huanan prerainy season. The shading indicates the terrain height (unit: m).

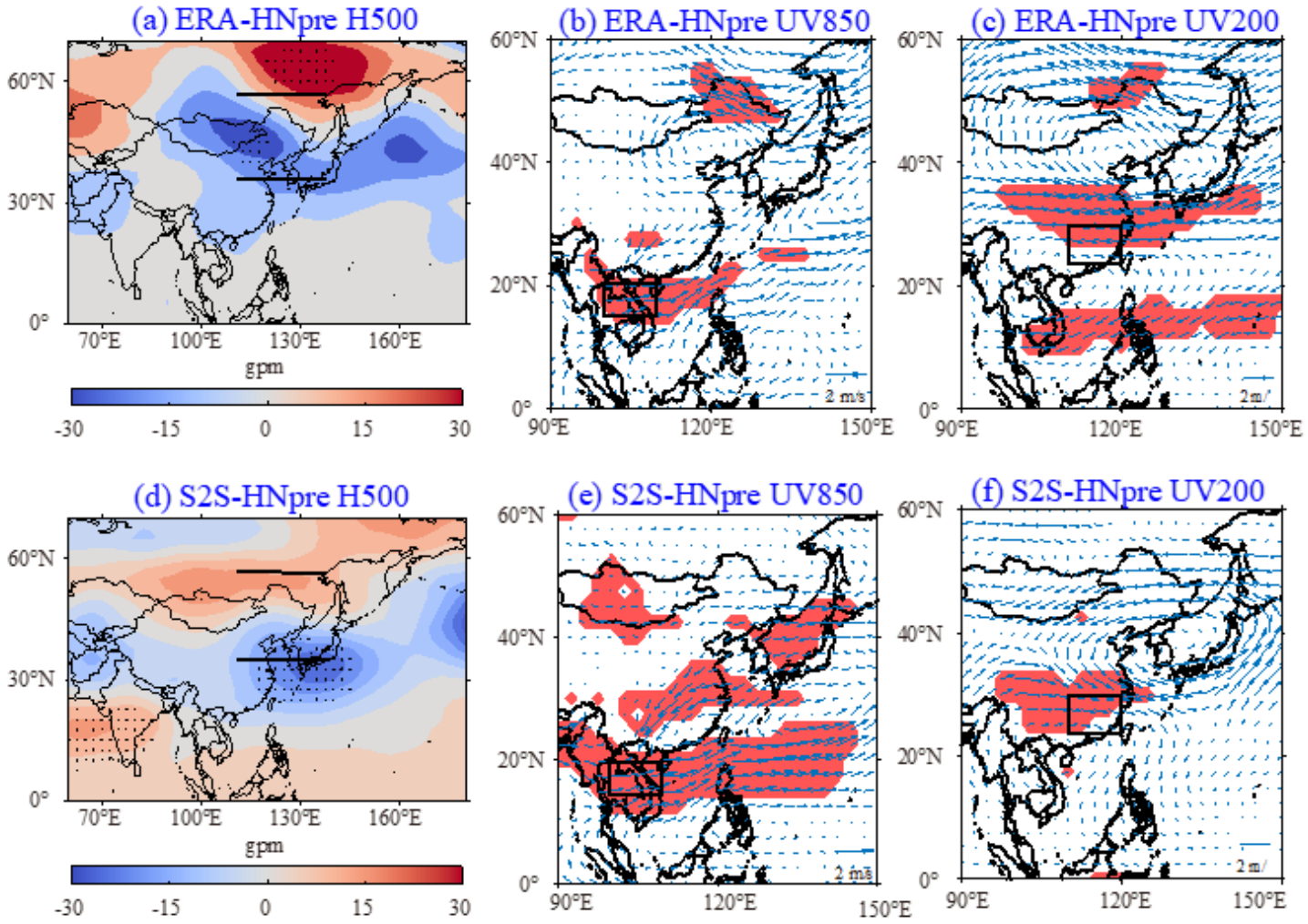

Figure 4

Regression of the 500 hPa height anomaly field (a), the 850 hPa wind anomaly field (b) and the 200 hPa wind anomaly field (c) with the precipitation index during the Huanan rainy season for the ERA-Interim product. d, e and f are the same as a, b and c but for ECMWF predictions. The dots in a, d and the red shading in b, e, c, f represent areas significant at the 95% confidence level.

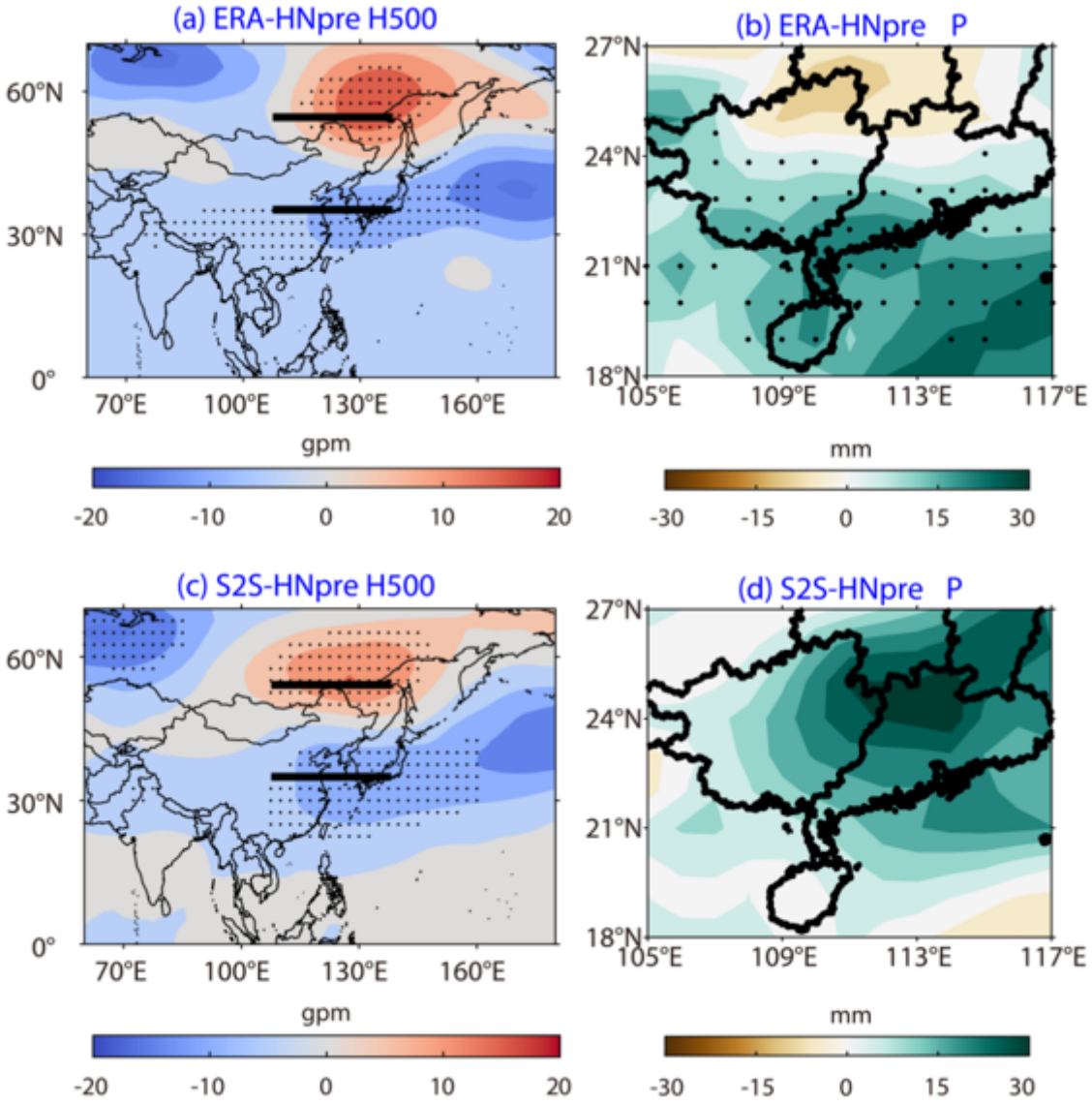

Figure 5

Regression of the 500 hPa height anomaly field (a) and the precipitation field (b) with the BHP index during the Huanan prerainy season based on the ERA-Interim product. c and d are the same as a and b but for ECMWF predictions. The dots represent areas with significant values at the 95% confidence level.

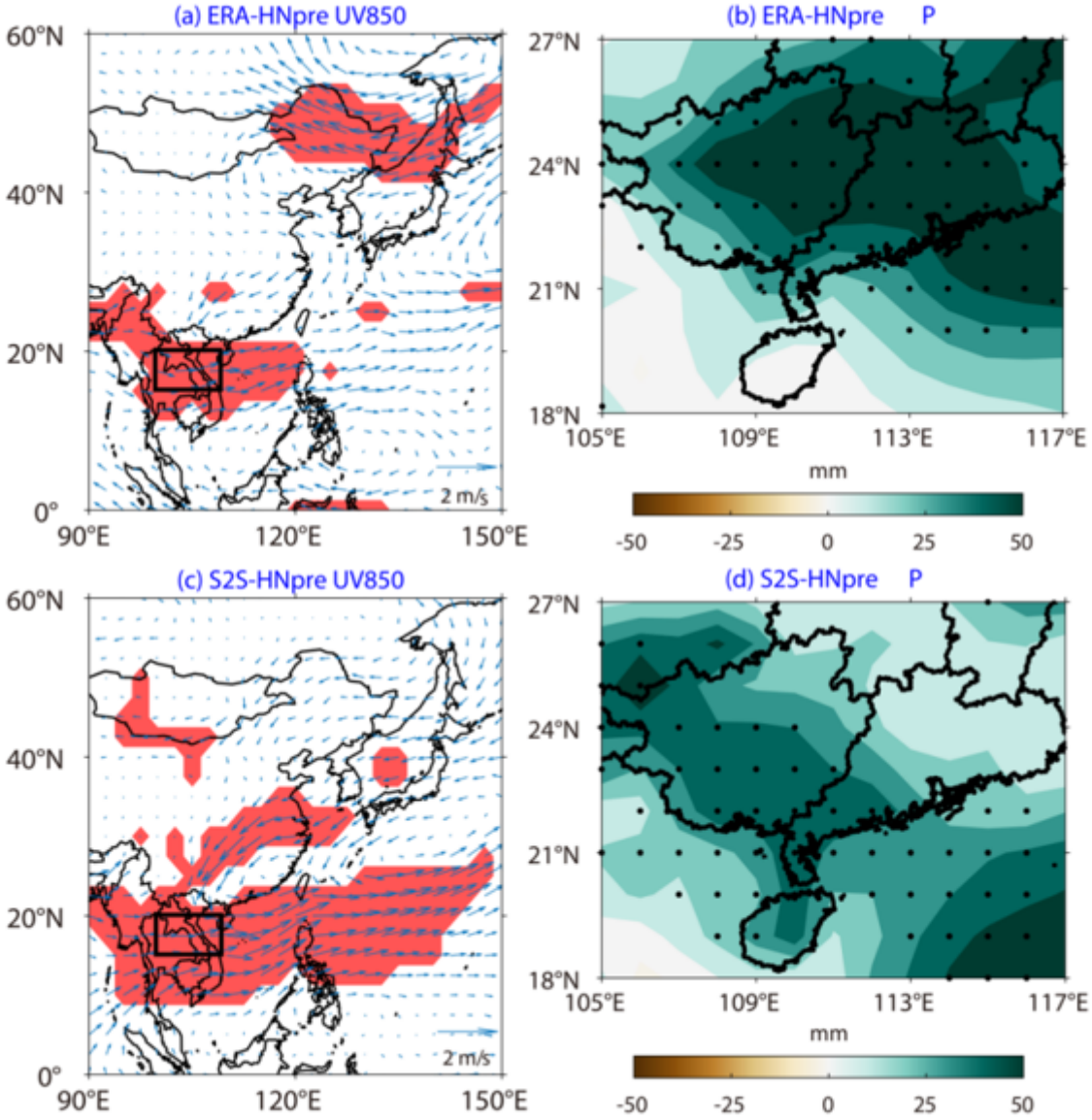

Figure 6

Regression of the 850 hPa wind anomaly field (a) and the precipitation field (b) onto the 850 hPa wind index during the Huanan prerainy season based on the ERA-Interim product. c and d are the same as a and b but for ECMWF predictions. The red shading in a and c and the dots in b and d represent areas with values that are significant at the 95% confidence level.

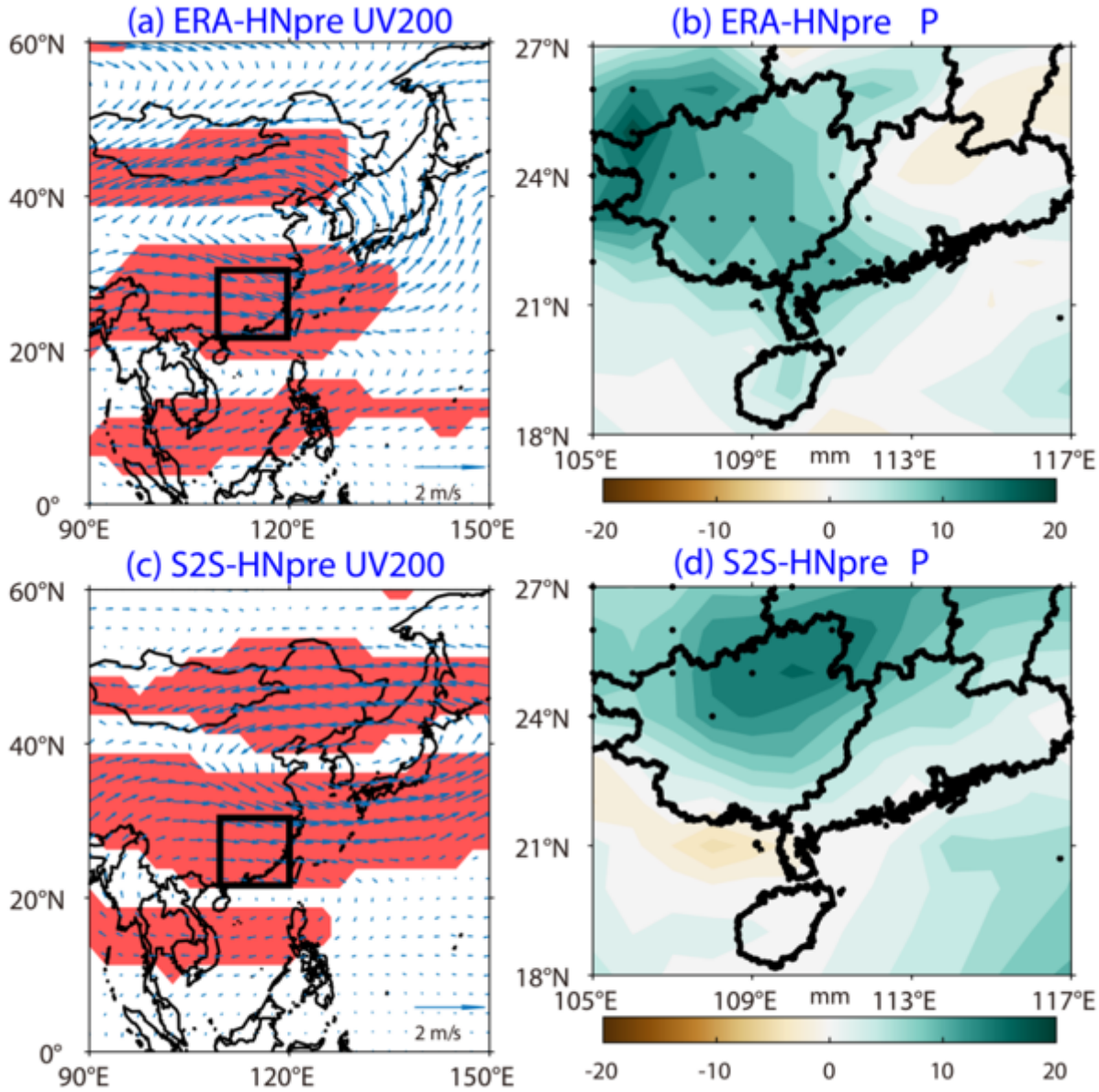

Figure 7

Regression of the 200 hPa wind field anomaly field (a) and the precipitation field (b) with the 200 hPa wind index during the Huanan prerainy season based on the ERA-Interim product. c and d are the same as a and b but for ECMWF predictions. The red shading in a and c and the dots in b and d represent areas with values that are significant at the 95% confidence level.

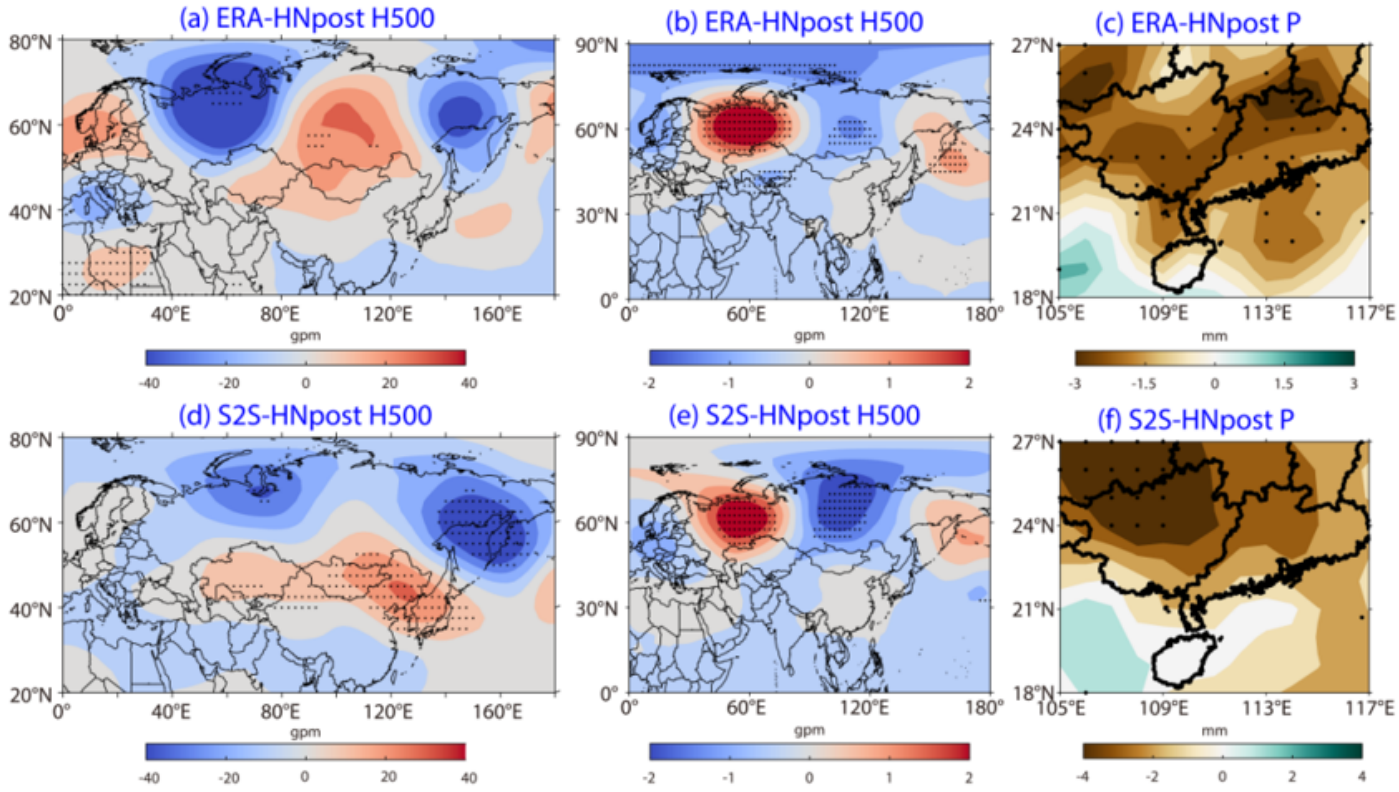

Figure 8

Regression of the 500 hPa height anomaly field (a) with the precipitation index and regression of the 500 hPa height anomaly field (b) and the precipitation field (c) with the EU index during the Huanan post-rainy season based on the ERA-Interim product. Panels d-f are the same as a-c but for ECMWF predictions. The dots represent areas with significant values at the 95% confidence level.

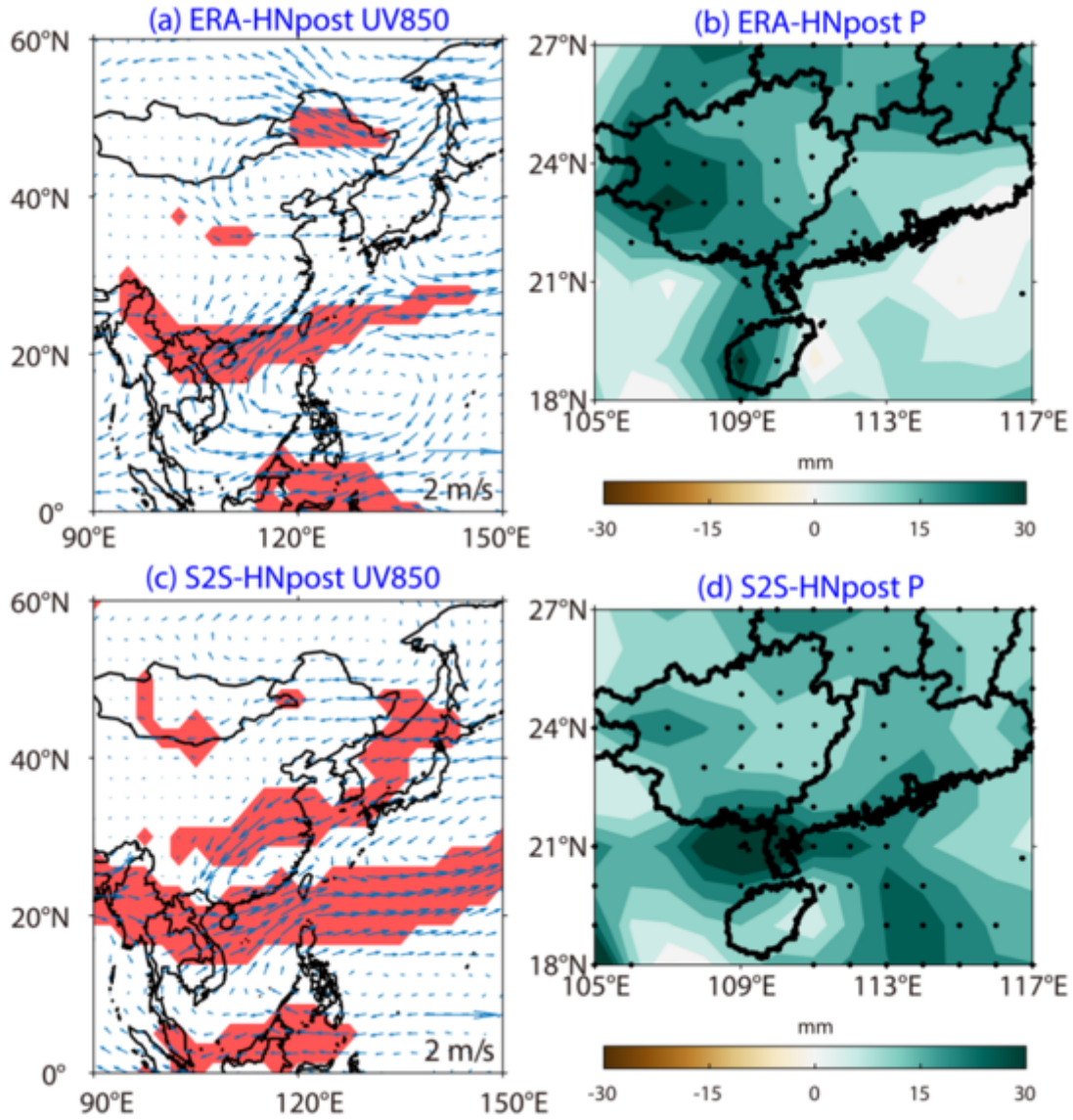

Figure 9

Regression of the 850 hPa wind anomaly field (a) and precipitation field (b) with the 850 hPa wind index during the Huanan post-rainy season based on the ERA-Interim products. Panels c and d are the same as panels a and b but for ECMWF predictions. The red shading in a and c and the dots in b and d represent areas with values that are significant at the 95% confidence level.

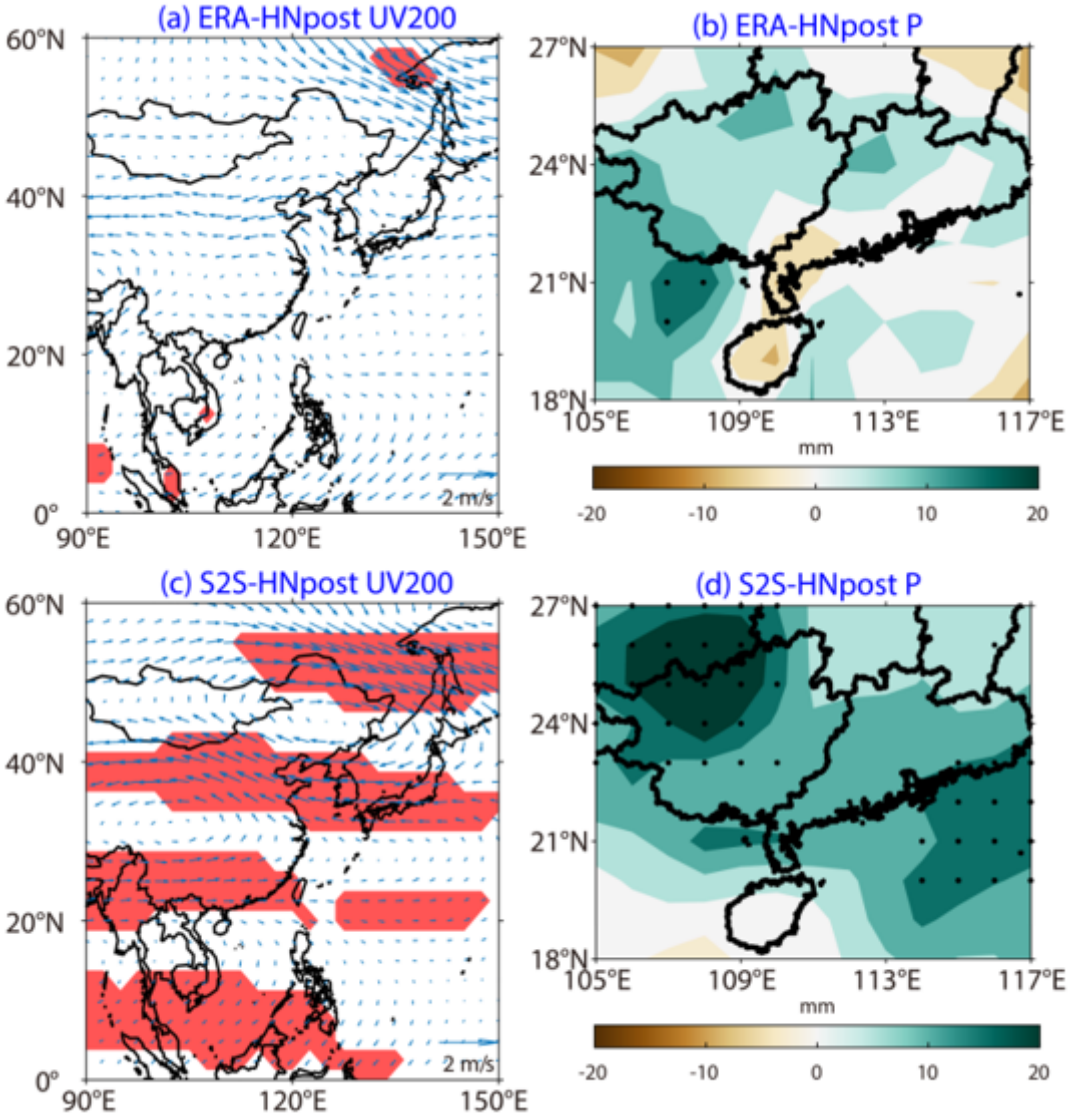

Figure 10

Regression of the 200 hPa wind field anomaly field (a) and the precipitation field (b) with the 200 hPa wind index during the Huanan post-rainy based on the ERA-Interim product. Panels c and d are the same as panels a and b but for ECMWF predictions. The red shading in a and c and the dots in b and d represent areas with values that are significant at the 95% confidence level.

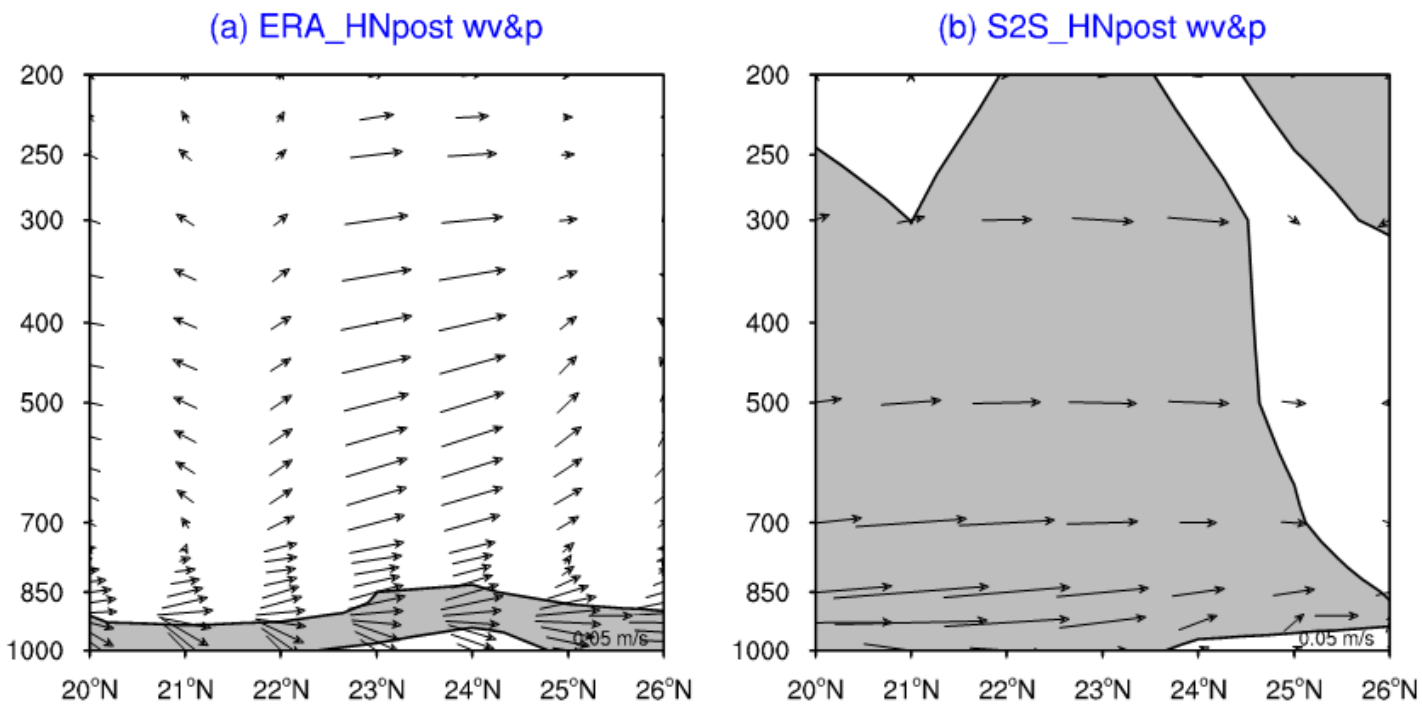

Figure 11

Regression of the vertical cross-section of the meridional wind anomaly field (v, -100 w) along 117°E and the precipitation index during the Huanan post-rainy season based on the ERA-Interim product (a). Panel b is the same as panel a but for ECMWF predictions. The shaded areas represent areas with values that are significant at the 95% confidence level.